J|A|C|S ARTICLES

Published on Web 04/01/2009

# Hydrophobic Dimerization and Thermal Dissociation of Perylenediimide-Linked DNA Hairpins

Mahesh Hariharan,[†] Yan Zheng,[†,§] Hai Long,[†,||] Tarek A. Zeidan,[†,⊥] George C. Schatz,[†] Josh Vura-Weis,[†] Michael R. Wasielewski,[†,‡] Xiaobing Zuo,[†,‡,¶] David M. Tiede,[†,‡] and Frederick D. Lewis*[,†]

*Department of Chemistry, Northwestern University, Evanston, Illinois 60208-3113, Chemistry Division, Argonne National Laboratory, Argonne, Illinois 60439, and Argonne-Northwestern Solar Energy Research (ANSER) Center*

Received January 16, 2009; E-mail: fdl@northwestern.edu

***Abstract:*** The structure and properties of hairpin-forming bis(oligonucleotide) conjugates possessing perylenediimide (PDI) chromophores as hairpin linkers have been investigated using a combination of spectroscopic and computational methods. These conjugates exist predominantly as monomer hairpins at room temperature in the absence of added salt and as head-to-head hairpin dimers in the presence of >50 mM NaCl. The hairpin dimer structure is consistent with the results of small-angle X-ray scattering in aqueous solution and molecular dynamics simulation. The structure of the nonconjugated PDI dimer in water is investigated using potential of mean force calculations. The salt dependence is attributed to increased cation condensation in the hairpin dimer vs monomer. Upon heating at low salt concentrations, the hairpin dimer undergoes sequential dissociation to form the monomer hairpin followed by conversion to a random coil structure; whereas at high salt concentrations both dissociation processes occur over the same temperature range. The monomer and dimer hairpins have distinct spectroscopic properties both in the ground state and excited singlet state. The UV and CD spectra provide evidence for electronic interaction between PDI and the adjacent base pair. Low fluorescence quantum yields are observed for both the monomer and dimer. The transient absorption spectrum of the dimer undergoes time-dependent spectral changes attributed to a change in the PDI−PDI torsional angle from ca. 20° in the Franck−Condon singlet state to ca. 0° in the relaxed singlet state, a process which occurs within ca. 40 ps.

## Introduction

Perylenediimide (PDI) and its derivatives have an unusual propensity to form dimers and aggregates and thus continue to attract interest as building blocks for multichromophoric assemblies.[1−4] The large $\pi$-faces of PDI render it highly hydrophobic; however, addition of water-solubilizing substituents[5,6] or conjugation with water-soluble polymers can impart solubility in aqueous solution.[7] Bis(oligonucleotide) conjugates possessing PDI linkers have been reported to form a variety of base-paired structures, including duplexes, triplexes, hairpins, and capped hairpins.[2,6,8−10] Novel thermophilic foldable oligomers possessing multiple PDI chromophores connected by disordered oligonucleotides have also been reported,[11] as have duplexes and hairpins in which a pendant PDI chromophore serves as a base pair surrogate.[12,13]

We have reported that bis(oligonucleotide) conjugate **1**, which possesses poly(dA)-poly(dT) base sequences connected by a PDI linker, forms a hairpin dimer in dilute aqueous buffer containing 100 mM NaCl (Scheme 1).[14,15] Molecular modeling suggests

[†] Northwestern University.
[§] Present address: PolyEra Corporation, Skokie, IL 60077.
[||] Present address: National Renewable Energy Laboratory, Computational Materials Science Center, Golden, CO 80401.
[⊥] Present address: Alkermes Inc., Cambridge, MA 02139.
[‡] Argonne National Laboratory.
[¶] Present address: National Cancer Institute, Frederick, MD 21702.

(1) Würthner, F.; Thalacker, C.; Diele, S.; Tschierske, C. *Chem.—Eur. J.* **2001**, *7*, 2245–2253.
(2) Li, A. D. Q.; Wang, W.; Wang, L. *Chem.—Eur. J.* **2003**, *9*, 4594–4601.
(3) (a) Würthner, F. *Chem. Commun.* **2004**, 1564–1579. (b) van der Boom, T.; Hayes, R. T.; Zhao, Y.; Bushard, P. J.; Weiss, E. A.; Wasielewski, M. R. *J. Am. Chem. Soc.* **2002**, *124*, 9582–9590. (c) Ahrens, M. J.; Sinks, L. E.; Rybtchinski, B.; Liu, W.; Jones, B. A.; Giaimo, J. A.; Gusev, A. V.; Goshe, A. J.; Tiede, D. M.; Wasielewski, M. R. *J. Am. Chem. Soc.* **2004**, *126*, 8284–8294.
(4) Tauber, M. J.; Kelley, R. F.; Giaimo, J. A.; Rybtchinski, B.; Wasielewski, M. R. *J. Am. Chem. Soc.* **2006**, *128*, 1782–1783.
(5) (a) Kohl, C.; Weil, T.; Qu, J. Q.; Müllen, K. *Chem.—Eur. J.* **2004**, *10*, 5297–5310. (b) Qu, J. Q.; Kohl, C.; Pottek, M.; Müllen, K. *Angew. Chem., Int. Ed.* **2004**, *43*, 1528–1531.
(6) Tang, T.; Peneva, K.; Müllen, K.; Webber, S. E. *J. Phys. Chem. A* **2007**, *111*, 10609–10614.
(7) Margineanu, A.; Hofkens, J.; Cotlet, M.; Habuchi, S.; Stefan, A.; Qu, J. Q.; Kohl, C.; Müllen, K.; Vercammen, J.; Engelborghs, Y.; Gensch, T.; De Schryver, F. C. *J. Phys. Chem. B* **2004**, *108*, 12242–12251.
(8) (a) Bevers, S.; Schutte, S.; McLaughlin, L. W. *J. Am. Chem. Soc.* **2000**, *122*, 5905–5915. (b) Abdalla, M. A.; Bayer, J.; Radler, J. O.; Müllen, K. *Angew. Chem., Int. Ed.* **2004**, *43*, 3967–3970. (c) Bayer, J.; Radler, J. O.; Blossey, R. *Nano Lett.* **2005**, *5*, 497–501.
(9) Rahe, M.; Rinn, C.; Carell, T. *Chem. Commun.* **2003**, 2120–2121.
(10) Ustinov, A. V.; Dubnyakova, V. V.; Korshun, V. A. *Tetrahedron* **2008**, *64* (7), 1467–1473.
(11) Wang, W.; Wan, W.; Zhou, H. H.; Niu, S. Q.; Li, A. D. Q. *J. Am. Chem. Soc.* **2003**, *125*, 5248–5249.
(12) Wagner, C.; Wagenknecht, H. A. *Org. Lett.* **2006**, *8*, 4191–4194.
(13) Zeidan, T. A.; Carmieli, R.; Kelley, R. F.; Wilson, T. M.; Lewis, F. D.; Wasielewski, M. R. *J. Am. Chem. Soc.* **2008**, *130*, 13945–13955.

 **10.1021/ja900347t CCC: $40.75** 

***Scheme 1.*** Monomer−Dimer Equilibrium for a PDI-Linked Hairpin

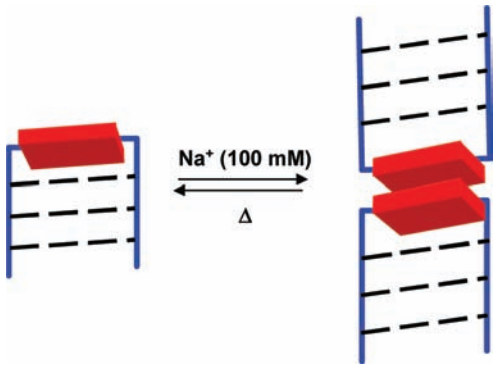


***Chart 1.*** Structures for the Base-Paired Hairpin Monomers **1** and **2** and for the PDI Hairpin Linker

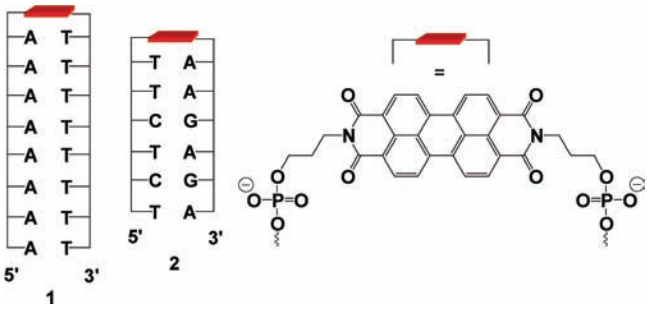


that the dimer adopts a head-to-head geometry in which the PDI linkers are $\pi$-stacked and aligned either parallel or antiparallel. There have been numerous reports of intramolecular PDI dimers.[1,2] To our knowledge, the hairpin conjugates provide the only example of the formation of a discrete PDI−PDI dimer which is not assembled by covalent bonding, hydrogen bonding, or multiple PDI−PDI interactions.[4,10,16,17] As such, they are free to adopt a dimer geometry without geometric constraints imposed by either covalent or noncovalent assembly.

We report here the results of our collaborative investigation of the structure and spectroscopic properties of the hairpin-forming PDI conjugates **1** and the structure of the related hairpin **2** (Chart 1). The monomer−dimer equilibrium for **1** is found to be dependent upon salt concentration and temperature, as well as the concentration of the conjugate. This conjugate exists predominantly as a monomeric hairpin at room temperature in aqueous buffer in the absence of added salt and as a hairpin dimer in the presence of added salt, with a threshold $Na^+$ concentration for dimer formation of ca. 10 mM. Thermal dissociation of the dimer at low salt concentrations occurs via a two-step mechanism, dimer dissociation followed by base pair dissociation, whereas at high salt concentrations both processes occur over the same temperature range. The monomer and dimer display distinct spectroscopic properties, both in their ground and excited states.

## Results

**Absorption Spectra.** Conjugates **1** and **2** were prepared following the procedure of Letsinger and Wu[18] as modified by

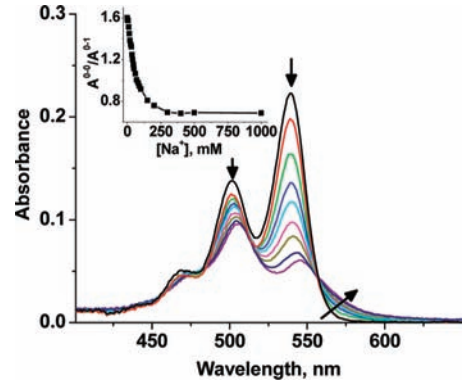


***Figure 1.*** NaCl concentration dependence of the absorption spectra of PDI conjugate **1** (1 $\mu$M) in 10 mM phosphate buffer (pH 7.2). Arrows show the effect of increasing NaCl concentration. Inset shows the ratio of vibronic bands ($A^{0-0}/A^{0-1}$) vs the NaCl concentration.

Rahe et al.[9] for the incorporation of the PDI linker.[19] The long-wavelength portion of the UV−vis absorption spectra of conjugate **1** in 10 mM sodium phosphate buffer in the absence and presence of added NaCl (0.005−1.1 M) are shown in Figure 1. The long-wavelength band is assigned to the PDI chromophore, whereas a shorter wavelength band (not shown) is assigned to overlapping absorption of PDI and the nucleobases.[20] The spectrum of the long wavelength band in buffer is similar to that of a soluble derivative of the PDI linker in dichloromethane solution and has a $A^{0-0}/A^{0-1}$ band intensity ratio of 1.4:1, characteristic of nonaggregated PDI derivatives.[21] Addition of NaCl red-shifts both the $A^{0-0}$ and $A^{0-1}$ bands, decreases their peak intensities, and causes pronounced tailing of the $A^{0-0}$ band toward long wavelengths. At high salt concentrations, the $A^{0-0}/A^{0-1}$ band intensity ratio asymptotically approaches a value of 0.65 characteristic of dimeric PDI (Figure 1, inset). The $A^{0-0}/A^{0-1}$ band intensity ratio in buffer is independent of the concentration of **1** (0.5−5.5 $\mu$M), indicating that the conjugate is predominantly in the form of the monomer. However, in the presence of 100 mM NaCl the band intensity ratio decreases with increasing concentration of **1** from a value of 0.78 for 0.5 $\mu$M **1** to 0.60 for 5.5 $\mu$M **1** (Figure 2).

The temperature dependence of the absorption spectra of **1** was determined in buffer and with added NaCl (0.005−1.0 M). The spectra obtained in buffer and with 1.0 M NaCl are shown in Figure 3a,b. Thermal dissociation profiles in the presence and absence of added 1.0 M salt determined both from the 260 nm absorption and $A^{0-0}/A^{0-1}$ band intensity ratios are shown in Figure 3c,d. The derivatives of the 260 nm thermal dissociation profiles provide values of $T_m = 40$ °C in buffer and 70 °C with 1.0 M NaCl. A weaker melting transition with $T_m \approx 50$ °C is also observed in the presence of salt, but not in its absence. The $A^{0-0}/A^{0-1}$ band intensity ratio decreases only slightly with increasing temperature in buffer, but is strongly temperature dependent in the presence of 1.0 M NaCl. The first derivative of this ratio provides a value of $T_m = 70$ °C, identical to the value obtained from the 260 nm data. A gradual increase in $A^{0-0}/A^{0-1}$ band intensity ratio is also observed at temperatures below the melting transition in the presence of 1.0 M NaCl (Figure 3d).

(14) Zheng, Y.; Long, H.; Schatz, G. C.; Lewis, F. D. *Chem. Commun.* **2005**, 4795–4797.
(15) Zheng, Y.; Long, H.; Schatz, G. C.; Lewis, F. D. *Chem. Commun.* **2006**, 3830–3822.
(16) Wang, Y. F.; Chen, Y. L.; Li, R. J.; Wang, S. Q.; Su, W.; Ma, P.; Wasielewski, M. R.; Li, X. Y.; Jiang, J. Z. *Langmuir* **2007**, *23*, 5836–5842.
(17) Seki, T.; Yagai, S.; Karatsu, T.; Kitamura, A. *J. Org. Chem.* **2008**, *73*, 3328–3335.
(18) Letsinger, R. L.; Wu, T. *J. Am. Chem. Soc.* **1995**, *117*, 7323–7328.
(19) The Experimental Section is available as Supporting Information.
(20) Sadrai, M.; Hadel, L.; Sauers, R. R.; Husain, S.; Kroghjespersen, K.; Westbrook, J. D.; Bird, G. R. *J. Phys. Chem.* **1992**, *96*, 7988–7996.
(21) Giaimo, J. A.; Lockard, J. V.; Sinks, L. E.; Scott, A. M.; Wilson, T. M.; Wasielewski, M. R. *J. Phys. Chem. A* **2008**, *112*, 2322–2330.

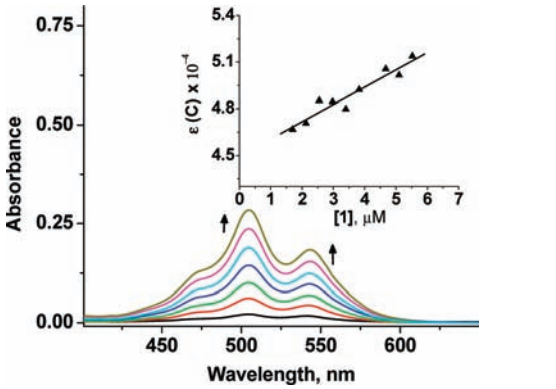


*Figure 2.* Concentration dependence of the absorption spectrum of PDI conjugate **1** (0.5−5.5 $\mu$M) in 10 mM phosphate buffer (pH 7.2) containing 100 mM NaCl. Inset shows the 505 nm molar absorbance vs concentration.

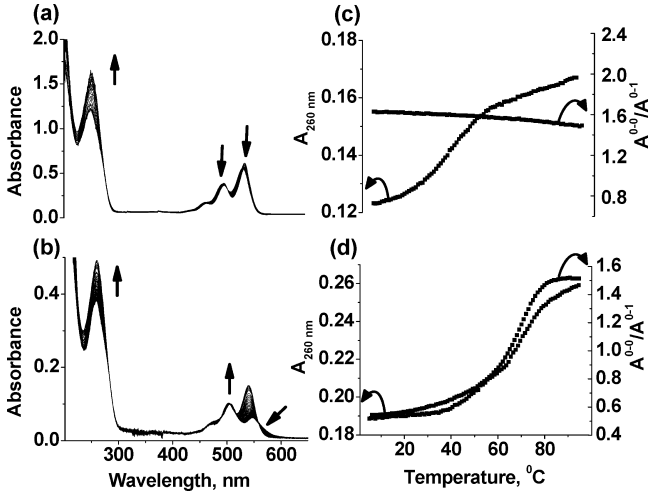


*Figure 3.* Temperature-dependent absorption spectra of PDI conjugate **1** (2.1 $\mu$M) in (a) 10 mM phosphate buffer (pH 7.2) and (b) buffer containing 1 M NaCl. Melting curves for (c) **1** (1.0 $\mu$M) in 10 mM phosphate buffer (pH 7.2) monitored at 260 nm (left axis) and the ratio $A^{0-0}/A^{0-1}$ (right axis) and (d) in buffer containing 1 M NaCl monitored at 260 nm (left axis) and the ratio $A^{0-0}/A^{0-1}$ (right axis).

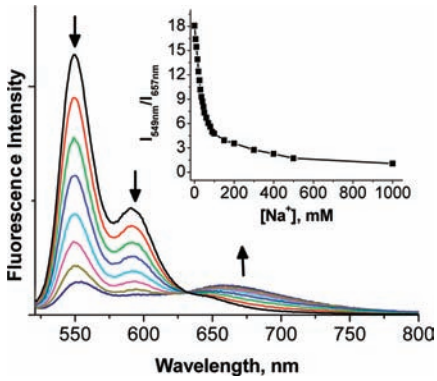


*Figure 4.* Effect of NaCl concentration (0−1 M) on the fluorescence emission spectra of PDI conjugate **1** (1 $\mu$M) in 10 mM phosphate buffer (pH 7.2). Inset shows the ratio of fluorescence intensities ($I_{549}/I_{657}$) versus the NaCl concentration (excitation wavelength 505 nm).

**Fluorescence Spectra.** The fluorescence spectra of **1** in buffer in absence and presence of added NaCl (0.005 to 1.1 M) are shown in Figure 4. The fluorescence excitation spectrum in buffer (Figure S1) has vibronic band maxima and relative

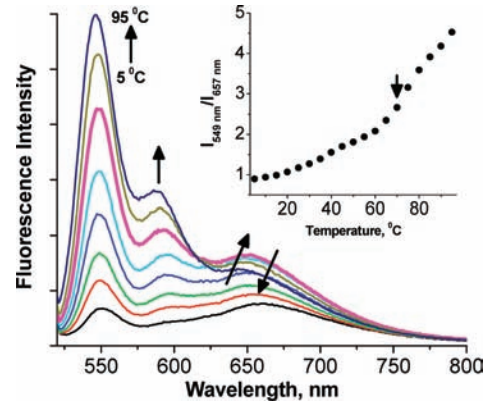


*Figure 5.* Temperature dependence of the fluorescence emission spectra of PDI conjugate **1** (1 $\mu$M) in 10 mM phosphate buffer (pH 7.2) containing 1 M NaCl. Inset shows the ratio of fluorescence intensities ($I_{549}/I_{657}$) versus the temperature (excitation wavelength, 505 nm). Bold trace and arrow in the inset show the temperature at which the maximum 657 nm emission intensity is observed.

intensities similar to those of the absorption spectrum in buffer (Figure 3a) and is assigned to the monomer. The fluorescence emission spectrum in buffer has a mirror image relationship to the absorption and fluorescence excitation spectrum with vibronic bands at 549, 591, and 655 nm and a $I_{549\ nm}/I_{657\ nm}$ band intensity ratio of 18. The fluorescence quantum yield of conjugate **1** in buffer at 20 °C is 0.009 ± 0.001.

Addition of NaCl results in reduced intensity of the 549 nm PDI monomer band intensity and a concomitant, but attenuated, increase in intensity of a broadband at 657 nm band with an isoemissive point at 632 nm (Figure 4). The 657 nm band is assigned to excimer emission of the excited singlet state of the ground-state dimer.[21] The ratio of 549/657 nm band intensities decreases with added salt (Figure 4, inset) and approaches a value of ca. 1.1 at high salt concentration. The fluorescence excitation spectrum in buffer with 1.0 M NaCl is emission wavelength dependent, spectra obtained at emission wavelengths of 600 and 657 nm resembling the absorption spectra of the monomer and dimer, respectively (Figure S1). The $I_{549\ nm}/I_{657\ nm}$ fluorescence band intensity ratio is dependent upon the concentration of **1** in 0.1 M NaCl (Figure S2), decreasing from 4.2 for 0.5 $\mu$M **1** to 1.8 for 5.5 $\mu$M **1**.

The temperature-dependent fluorescence spectra of conjugate **1** in the presence of added 1.0 M NaCl are shown in Figure 5. Increasing temperature results in an increase in the 549 nm band intensity. The 657 nm band intensity also increases with increasing temperature, attaining a maximum value at ca. 70 °C and then decreasing at higher temperature. The derivative of a plot of the $I_{549\ nm}/I_{657\ nm}$ band intensity ratio (Figure 5, inset) also provides a value of $T_m$ = 70 °C, identical to that obtained from UV melting (Figure 3d). Integration of the spectrum obtained at 20 °C shows that it consists of ca. 75% excimer emission centered at 657 nm and ca. 25% monomer emission at 549 nm with a total fluorescence quantum yield of ca. 0.001.

**Circular Dichroism Spectra.** The circular dichroism (CD) spectra of **1** in buffer in the absence and presence of 1.0 M NaCl are shown in Figure 6a,b. The short-wavelength regions of the CD spectrum display positive bands at 280 and 220 nm and a negative band at 246 nm, characteristic of poly(dA)-poly(dT) duplexes and hairpins.[22] The CD spectrum at 20 °C

(22) Lewis, F. D.; Wu, Y.; Liu, X. *J. Am. Chem. Soc.* **2002**, *124*, 12165–12173.

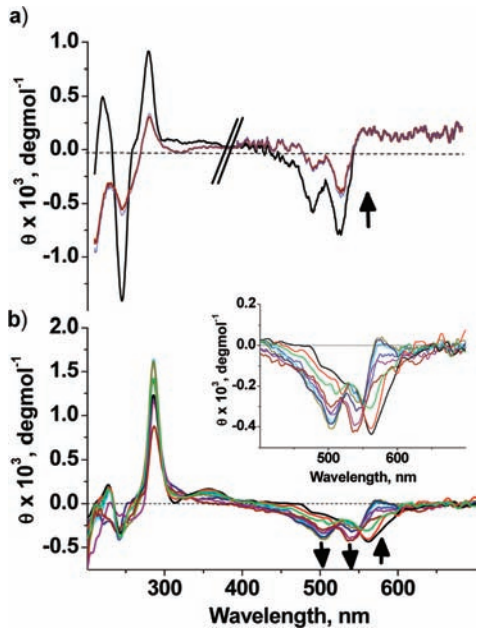


***Figure 6.*** Temperature dependence (5−85 °C) of the CD spectra of PDI conjugate **1** (5 $\mu$M) (a) in 10 mM phosphate buffer (pH 7.2) and (b) in buffer containing 1 M NaCl. Long-wavelength portion of the spectra in (a) is multiplied by 2.

in buffer displays a negative band at long wavelengths (Figure 6a) with vibronic band positions and relative intensities similar to those for the long wavelength absorption band of the monomer in buffer (Figure 1). The intensity of both the 260 and 535 nm CD bands in buffer decrease with increasing temperature (Figure S3a), providing a CD melting temperature of ca. 40 °C, similar to those obtained from UV melting (Figure 3c).

The CD spectrum in the presence of 1.0 M NaCl has a negative band at 567 nm and a positive band at 350 nm (Figure 6b), neither of which are observed in the absence of added salt. The 567 nm band coincides with the tail of the absorption spectrum with added salt (Figures 1 and 3a) and is assigned to the hairpin dimer. The long wavelength CD band displays complex temperature dependence, undergoing a change in band shape between 5 and 35 °C to provide a spectrum similar to that of the absorption spectrum of the PDI dimer in the presence of added salt (Figure 3b). At higher temperatures, this spectrum is replaced by one resembling that of the PDI monomer hairpin (Figure 3a). The CD melting profiles determined both at 260 and 543 nm (Figure S3b,c) display a marked decrease in rotation near 70 °C, the melting temperature obtained from UV and fluorescence data. The rotational strength increases with increasing temperature below the melting temperature.

**Transient Absorption Spectra.** Femtosecond time-resolved transient absorption spectra of the conjugate **1** in buffer in the absence and presence of 1.0 M NaCl were obtained using 505 nm, 130 fs laser pump pulses (Figure 7). The transient spectra between 440−800 nm and 0−6 ns were subjected to singular value decomposition (SVD) and global fitting using a sum of exponentials to obtain the principal kinetic components and their associated spectra (insets, Figure 7).[23] The transient spectra in the absence of added salt (Figure 7a) display a positive band at 705 nm and negative bands around 500, 540, and 600 nm. On

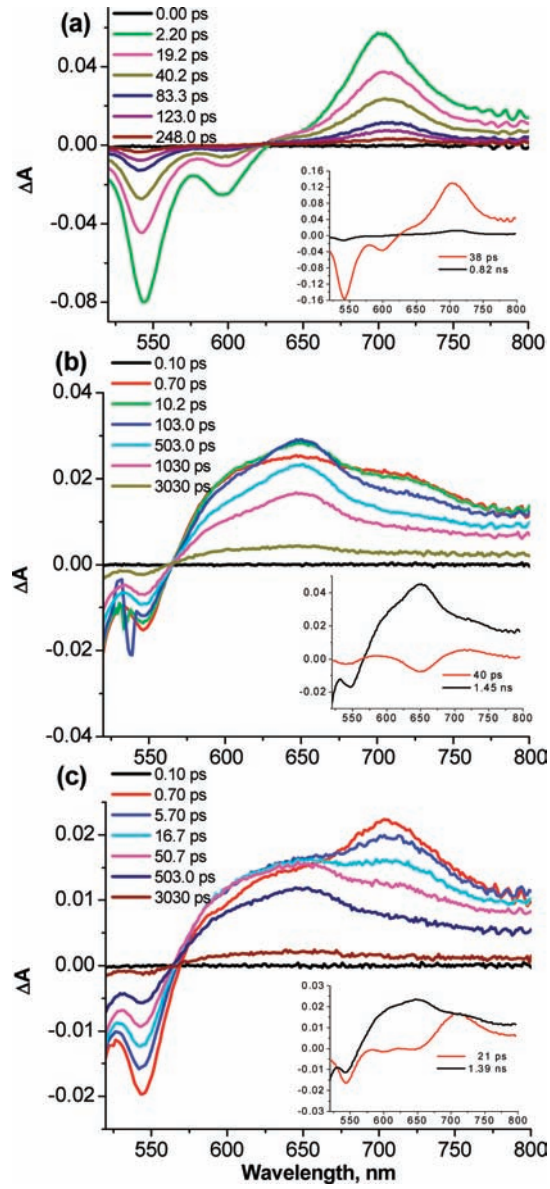


***Figure 7.*** Transient absorption spectra of PDI conjugate **1** in 10 mM phosphate buffer containing with no added salt (a) and with 1 M NaCl measured at (b) 20 and (c) 70 °C recorded at various intervals (ps) following excitation with 505 nm, 130 fs laser pulses. Insets: spectra associated with the kinetic components obtained by global analysis.

the basis of a comparison with the transient spectrum for the conjugate $T_6$-PDI-$T_6$,[24] the negative bands are assigned to ground-state depopulation (540 nm) and stimulated emission (600 nm), while the positive band is assigned to absorption of monomeric $^{1*}$PDI. The data analysis yields two principal kinetic components with decay times of 38 ps (91%) and 0.82 ns (9%) having similar associated spectra. The 38 ps component is assigned to the decay of monomeric $^{1*}$PDI. The very minor 0.82 ns component is most likely due to a small amount of structurally altered hairpin.

The transient spectra of **1** in the presence of 1 M NaCl at 20 and 70 °C are shown in panels b and c of Figure 7, respectively. In each case, immediately following the laser pulse the spectra display a negative band at 540 nm assigned to ground-state

(23) *Surface Xplorer*; Ultrafast Systems LLC: Sarasota, FL.

(24) Carmieli, R.; Zeidan, T. A.; Kelley, R. F.; Mi, Q.; Lewis, F. D.; Wasielewski, M. R. J. Phys. Chem. B, ASAP.

depopulation and a broad positive band at 570−800 nm. At 20 °C, the 570−800 nm absorption narrows rapidly ($\tau_1 = 40$ ps) into a band having a maximum near 650 nm. This rapid narrowing is consistent with the spectrum associated with $\tau_1$ (inset, Figure 7b) in which the minimum near 650 nm indicates that this band rises with $\tau_1$, while the positive $\Delta A$ bands on either side of 650 nm decay with $\tau_1$. The time scale of the observed spectral narrowing is sufficiently slow that it most likely does not result from vibrational cooling. The 650 nm band then decays to $\Delta A = 0$ with $\tau_2 = 1.45$ ns with no significant band shape changes. The 650 nm spectrum is assigned to the excimer-like state of PDI ($^{1*X}PDI_2$) that results from dimerization of **1** in the presence of 1 M NaCl at 20 °C. This assignment is based on similar photophysical behavior observed in covalent, cofacial PDI dimers.[21] At 70 °C, SVD and global analysis once again yield two principal spectra associated with $\tau_1 = 21$ ps and $\tau_2 = 1.39$ ns kinetic components. The spectrum associated with the short component shows a distinct maximum at 709 nm, which is only slightly red-shifted from that observed for monomeric $^{1*}$PDI in **1** with no NaCl present, and therefore is also assigned to that species. The spectrum of the long component has a broader 650 nm maximum and is very similar to that of **1** in the presence of 1 M NaCl at 20 °C, so that it is assigned to $^{1*X}PDI_2$ as well. It is important to note that, unlike the data obtained at 20 °C, the spectrum associated with the 21 ps component of **1** at 70 °C does not have a negative feature at 650 nm, so that the 650 nm band does not appear as the 709 nm band decays. The two kinetic components and their associated spectra are therefore assigned to the parallel decay of $^{1*}$PDI and $^{1*X}PDI_2$ that are both present in solution at the time of the laser pulse. The transient decays appear to be largely complete on the 6 ns time scale of our measurements. Attempts to detect longer-lived transients from **1** using a nanosecond pulsed laser apparatus with an instrument response time of ca. 7 ns were unsuccessful.[13]

**Solution X-ray Scattering of a Hairpin Dimer.** The solution structure of the PDI-linked hairpin **2** (Chart 1) in aqueous buffer containing 0.1 M NaCl was investigated by means of solution X-ray scattering using a high-flux synchrotron source (Advanced Photon Source, Argonne National Laboratory). A base pair domain consisting of four A−T base pairs and two G−C base pairs was employed for this study in order to minimize the possible effects of end-fraying. The linearity of the Guinier plot (Figure S4) indicates that sample is monodisperse with respect to size, having a radius of gyration of 15.5 ± 0.2 Å. An ab initio procedure for reconstructing the domain structure of the hairpin dimer using the DAMMIN program was employed to obtain the structure shown in Figure 8.[25] The dimensions of this cylindrical structure are ca. 48 × 20 Å$^2$.

**Molecular Modeling of the Hairpin Dimer.** We have previously reported the use of molecular dynamics (MD) simulations to obtain averaged structures for the dimer of hairpin **1**.[14] The base pair domain of **1** was truncated to three base pairs to reduce the time required for simulations and the hairpin dimer was constructed by assembling two monomers in head-to-head fashion. MD simulations provided averaged hairpin structures in which the hairpins either parallel (Figure 9b) or antiparallel (not shown) to each other. Both the parallel and antiparallel structures have shallow potential energy surfaces with respect to rotation about the axis connecting the centers of the two PDI chromophores with maximum populations at torsional angles of ca. ±20° with respect to the average angles of 4° and 180° for the parallel and antiparallel structures, respectively (Figure S5).

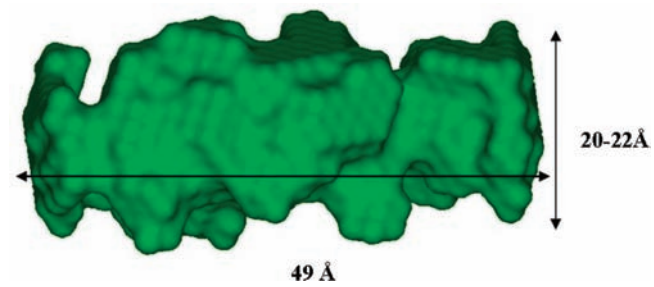


***Figure 8.*** Structure of hairpin dimer formed by PDI conjugate **2** in 10 mM phosphate buffer containing 100 mM NaCl determined by small-angle X-ray scattering.

The potential of mean force (PMF) of the interactions of two nonconjugated PDI molecules in aqueous solution is calculated using MD simulations and the umbrella sampling method. The computational details are presented in the Supporting Information. The angular dependence of the PMF plot for the PDI dimer is shown in Figure 10a. The PDI molecule has $D_{2h}$ symmetry so that only the PMF angular function from 0° to 90° is calculated. The distance dependence of the PMF for the PDI dimer is shown in Figure 10b.

## Discussion

**Structure and Spectroscopy of the PDI Hairpin Monomer.** MD simulation of the structure of a single PDI-linked hairpin possessing a truncated three-base pair stem in water shows that it adopts a normal B-DNA base pair domain with the PDI chromophore $\pi$-stacked with the adjacent base pair (Figure 9a). Similar structures have previously been observed for several hairpins having arene-dicarboxamide linkers.[26,27] As seen in the end on view (Figure 9a) the hydrophobic face of the PDI chromophore is substantially larger than the adjacent A−T base pair.

Formation of a base-paired monomer hairpin structure in the absence of added NaCl is consistent with the electronic spectra of **1**. The UV−vis absorption spectrum of **1** in buffer (Figures 1 and 3a) displays a vibronic band progression in which the $A^{0-0}/A^{0-1}$ band intensity ratios is ca. 1.4:1, characteristic of the PDI monomer.[21] The long-wavelength region of the CD spectrum of **1** in buffer (Figure 6a) displays a weak negative band with maxima that coincide with those of the absorption spectrum. Similar CD spectra have been reported for hairpins possessing arene dicarboxamide linkers which do not form hairpin dimers.[28] These spectra are attributed to the induced CD of the achiral linker in the chiral environment of the DNA hairpin.[22,29] The 260 nm UV thermal dissociation profile for **1** in buffer (Figure 3c) displays a single melting transition with $T_m = 40$ °C and ca. 28% hypochromism, a value similar to that for melting of a stilbene-linked poly(dT)/poly(dA) hairpin.[18] The 269 nm CD melting profile (Figure S3a) also displays a single

(25) Svergun, D. I. *Biophys. J.* **1999**, *77*, 2896–2896.
(26) Egli, M.; Tereshko, V.; Mushudov, G. N.; Sanishvili, R.; Liu, X.; Lewis, F. D. *J. Am. Chem. Soc.* **2003**, *125*, 10842–10849.
(27) Lewis, F. D.; Zhang, L.; Kelley, R. F.; McCamant, D.; Wasielewski, M. R. *Tetrahedron* **2007**, *63*, 3457–3464.
(28) Lewis, F. D.; Zhang, L.; Liu, X.; Zuo, X.; Tiede, D. M.; Long, H.; Schatz, G. C. *J. Am. Chem. Soc.* **2005**, *127*, 14445–14453.
(29) Ardhammar, M.; Kurucsev, T.; Nordén, B. In *Circular Dichroism, Principles and Applications*; Berova, N., Nakanishi, K., Woody, R. W., Eds.; Wiley-VCH: New York, 2000; Vol. 74 pp 1−768.

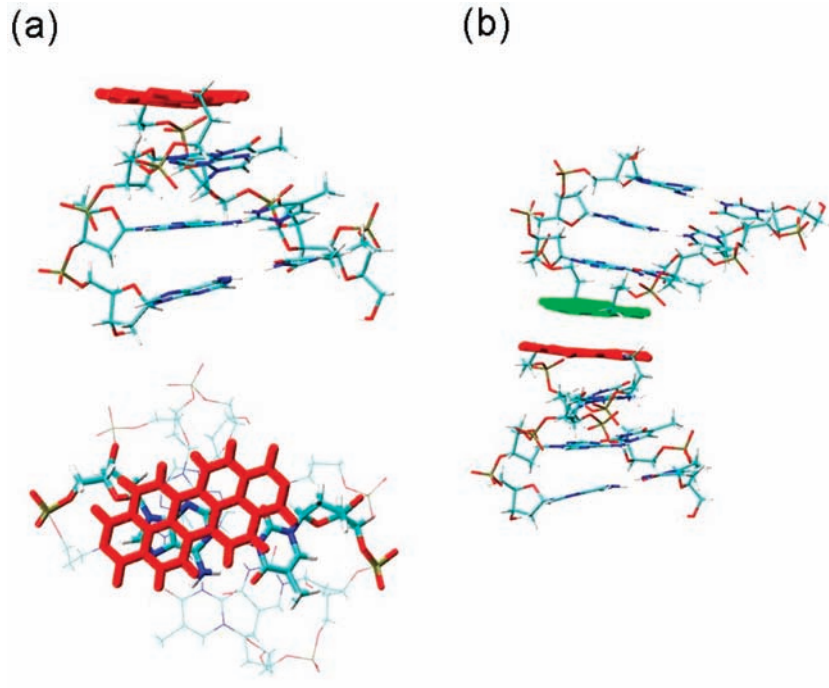


***Figure 9.*** Molecular dynamics simulations of (a) the monomer hairpin side-view and top-view and (b) hairpin dimer of **1**.

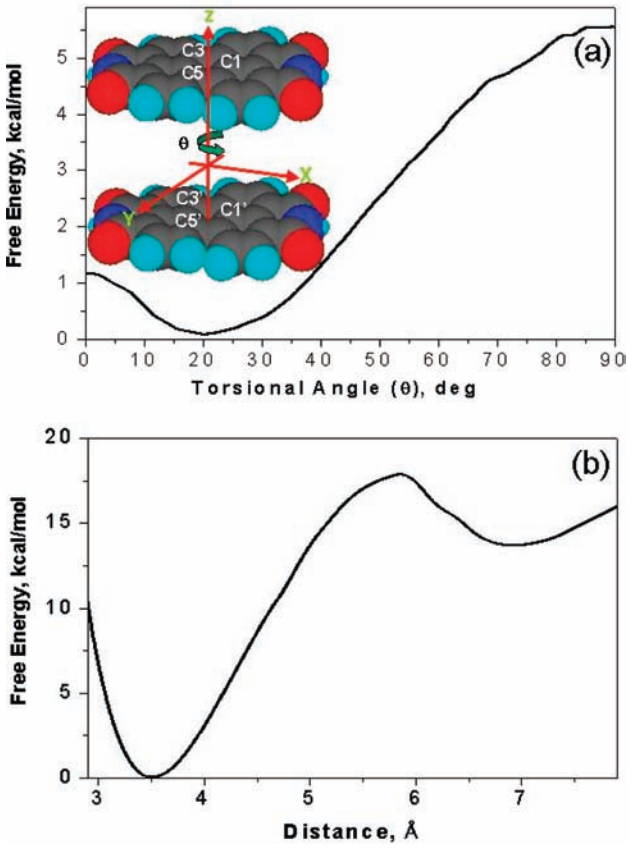


***Figure 10.*** Calculated free energy of the PDI dimer in water (a) vs the torsional angle between two PDI molecules and (b) vs the plane-to-plane distance between the two PDI molecules.

transition with no evidence for premelting, in accord with a simple two-state model for thermal base pair dissociation.

The fluorescence spectrum of **1** in buffer (Figure 3) has a mirror image relationship to the absorption and fluorescence excitation spectra. The fluorescence quantum yield is ca. 100-fold lower than that for an unconjugated PDI monomers in organic solvents ($\Phi_{fl} = 9 \times 10^{-3}$ vs $\Phi_{fl} \approx 1.0$).[21] The transient absorption spectrum of **1** in buffer has a symmetric band at 705 nm (Figure 7a) and resembles that of the PDI monomer singlet state rather than the broader spectrum of its anion radical.[13] The major component of the transient decay occurs with $\tau_1 = 39$ ps. The low fluorescence quantum yield and short transient decay time for **1** are indicative of quenching of singlet PDI by adjacent A−T base pairs. Quenching of PDI fluorescence by covalently attached oligonucleotides has been attributed to electron transfer processes in which singlet PDI serves as an electron acceptor and a purine base (adenine or guanine) serves as electron donor.[13] Rapid charge recombination of the resulting radical ion pair (inverted kinetics) can account for our failure to observe the PDI anion radical.[24,27]

**Structure of the Hairpin Dimer and the PDI Dimer in Water.** In our preliminary study of the PDI conjugate **1**, the formation of a hairpin dimer in aqueous solutions containing 1.3 $\mu$M **1**, 10 mM phosphate buffer and 100 mM NaCl was proposed on the basis of the inverted $A^{0-0}/A^{0-1}$ vibronic band intensity ratio.[14] Direct evidence for hairpin dimer formation in similar solution conditions is provided by the structure of the conjugate **2** (Chart 1) derived from small-angle X-ray scattering measurements (Figure 8). The dimensions of the cylindrical structure are ca. 48 × 20 Å$^2$. The length is consistent with the formation of the head-to-head dimer of **2** having a normal B-DNA $\pi$-stacking distance between base pairs, the two PDIs, and each PDI and its proximate base pair (13 × 3.6 Å = 46.8 Å) and the diameter is similar to that for B-DNA duplex structures.[26]

Molecular modeling of the head-to-head dimer of **1** provides the structure shown in Figure 9b in which the two PDI units form a sandwich-type dimer with a plane-to-plane distance of 3.5 Å, similar to the rise of B-DNA. The PDI electronic transition dipoles can be either parallel or antiparallel because of the helicity of the base pair domains. The average torsional

angles between PDI long axes are approximately 0° and 180° as a consequence of similar populations having torsional angles displaced ±20° from the average values (Figure S5). This value is somewhat smaller than the values of ca. 30° obtained from gas phase quantum mechanical calculations for the PDI dimer.[30−32]

Further information about the structure of the PDI dimer in water is provided by PMF calculations for the nonconjugated dimer. As seen in Figure 10a, the free energy minimum for the dimer occurs for a torsional angle of 20.5°. This can be explained by a balance between the hydrophobic and electrostatic interactions. The hydrophobic interactions are minimized in a perfect sandwich conformation with $\theta = 0°$. However, the interatomic distance between each pair of atoms is at a minimum in this conformation, thus maximizing the electrostatic repulsion energy. As a trade-off, the free energy minimum is located at 20.5° instead of 0°. Nevertheless, the barrier at 0° is around 1 kcal/mol or ∼2 kT at 300 K, which means that the torsional angle can easily change from negative to positive. At angles greater than 20.5°, the free energy increases to a maximum value of ca. 5 kcal/mol at 90° where overlap of the PDIs is at the minimum. The angular PMF plot of the PDI dimer shows a very broad well between ±40°, which defines the range of motions to be expected for the equilibrium structure.

The free energy minimum in the plot of free energy vs plane-to-plane separation (Figure 10b) occurs at 3.5 Å, similar to the optimal vertical distance between adjacent DNA base pairs (3.4 Å) or benzene dimers (3.5 Å).[33] The free energy increases significantly at shorter distances due to Pauli repulsion and at longer distance, owing to decreased orbital overlap. The plot has a maximum at 5.9 Å with a peak free energy of 17.9 kcal/mol. After this maximum, there is secondary minimum at 6.9 Å with a free energy of 13.7 kcal/mol. When the separation distance is larger than 6.9 Å, the free energy again increases. This oscillatory character has been observed in PMF plots for the benzene dimer[33] and a benzene−glucose complex[34] and is attributed to "squeezing" out layers of organized water on the molecule surface when the two molecules approach. The distance between minima roughly equals the solvent molecular diameter and these oscillations typically damp out after a few periods. This oscillatory character makes it difficult to calculate the free energy of the fully separated PDI dimer in bulk solution. But even if we take the value at the 6.9 Å minimum as the bulk free energy value, the depth of the primary minimum is 13.7 kcal/mol, significantly larger than the depth of the primary minimum for the benzene−benzene interaction (0.5 kcal/mol),[33] which indicates a stronger interaction between PDI molecules than benzene molecules.

The PMF calculations show that there is a strong attraction between PDI molecules in water and that the PDI dimer prefers to be stacked with a torsional angle around ±20°. However, we have imposed geometry restraints in these calculations (see Supporting Information for details), which could introduce artifacts. The actual binding affinity should also include contributions from other orientations.

**Spectroscopy of the Hairpin Dimer.** The UV spectra of the hairpin dimer obtained at high salt concentrations display inverted $A^{0-0}/A^{0-1}$ vibronic band intensities when compared to the spectra of the monomer in the absence of added salt (Figures 3a,b). In addition, the spectra of the dimer display red-shifted vibronic maxima and long-wavelength tailing. Qualitatively similar differences between PDI monomer and dimer absorption spectra have been predicted by Würthner et al.[30] and observed in organic solvents by Li[35,36] and Yagai[17] and their co-workers for intramolecular PDI dimers connected with flexible linkers and by Wasielewski et al. for a rigid PDI dimer.[21] The long-wavelength tailing in the spectrum of the hairpin dimer is more pronounced than is the case for covalent dimers in organic solvents and more nearly resembles the spectra of higher aggregates vs dimers.[37] Tailing is also observed in the 280 nm absorption band of the hairpin dimer under high salt conditions.

The long-wavelength portion of the CD spectrum of **1** at high salt concentrations displays a negative band at 560 nm and a positive band at 350 nm, wavelengths corresponding to the long-wavelength tails in the absorption spectra rather than the absorption maxima. We previously noted the absence of a strong bisignate CD Cotton effect in the spectrum of the hairpin dimer.[14] Exciton coupling between two $\pi$-stacked PDI chromophores is observed in duplex structures and was expected for the hairpin dimer. However, the presence of equal populations of dimers in the two conformational minima with torsional angles of ±20° (Figure S6) can account for the absence of PDI-PDI exciton coupling.[38] Both the tailing of the 280 and 550 nm bands observed in the UV spectra and the corresponding CD band maxima plausibly result from interactions of the PDI transition dipoles with the induced dipoles of the neighboring A−T base pairs. For transitions at the low-frequency edge of an absorption band, the induced dipole will always be in phase with the transition dipole, resulting in enhanced absorption in the red-edge of the absorption band.[39] The torsional angle for the dipole, induced-dipole interaction between the individual PDI chromophores and the adjacent A−T base pair should be the same in both hairpins, resulting in enhancement of the CD intensity at the red-edge of both the 280 and 550 nm bands.

The fluorescence spectrum of **1** at high salt concentrations (Figure 4) displays a broad weak band at 657 nm assigned to the singlet excimer based on analogy with the broad long wavelength emission observed for covalent PDI dimers and aggregates in nonaqueous solution.[21,36] The excimer fluorescence quantum yield is significantly smaller than that of the cofacial PDI dimer studied by Wasielewski, et al. ($\Phi_{fl} \approx 5 \times 10^{-4}$ vs $\Phi_{fl} = 0.02$).[21] A decrease in fluorescence quantum yield for nonconjugated PDI excimers vs monomers is commonly observed and attributed to enhanced nonradiative decay, a consequence of enhanced vibronic coupling. Very weak short-

(30) Seibt, J.; Marquetand, P.; Engel, V.; Chen, Z.; Dehm, V.; Wurthner, F. *Chem. Phys.* **2006**, *328*, 354–362.
(31) Clark, A. E.; Qin, C.; Li, A. D. Q. *J. Am. Chem. Soc.* **2007**, *129*, 7586–7595.
(32) Fink, R. F.; Seibt, J.; Engel, V.; Renz, M.; Kaupp, M.; Lochbrunner, S.; Zhao, H. M.; Pfister, J.; Würthner, F.; Engels, B. *J. Am. Chem. Soc.* **2008**, *130*, 12858–12859.
(33) Chipot, C.; Jaffe, R.; Maigret, B.; Pearlman, D. A.; Kollman, P. A. *J. Am. Chem. Soc.* **1996**, *118* (45), 11217–11224.
(34) Palma, R.; Himmel, M. E.; Brady, J. W. *J. Phys. Chem. B* **2000**, *104* (30), 7228–7234.
(35) Wang, W.; Li, L. S.; Helms, G.; Zhou, H. H.; Li, A. D. Q. *J. Am. Chem. Soc.* **2003**, *125*, 1120–1121.
(36) Han, J. J.; Shaller, A. D.; Wang, W.; Li, A. D. Q. *J. Am. Chem. Soc.* **2008**, *130*, 6974–6982.
(37) Chen, Z.; Stepanenko, V.; Dehm, V.; Prins, P.; Siebbeles, L. D. A.; Seibt, J.; Marquetand, P.; Engel, V.; Wurthner, F. *Chem.—Eur. J.* **2007**, *13*, 436–449.
(38) (a) Boiadjiev, S. E.; Anstine, D. T.; Lightner, D. A. *J. Am. Chem. Soc.* **1995**, *117*, 8727–8736. (b) Person, R. V.; Peterson, B. R.; Lightner, D. A. *J. Am. Chem. Soc.* **1994**, *116*, 42–59.
(39) (a) Tinoco, I. *Adv. Chem. Phys.* **1962**, *4*, 113. (b) Cantor, C. R.; Schimmel, P. R. *The Behavior of Biological Macromolecules*; W. H. Freeman: New York, 1980.

wavelength fluorescence bands similar to those assigned to the monomer are also observed at high salt concentrations (Figure 4). The fluorescence excitation spectra of the two emissions (Figure S1) correspond to the absorption spectra of the dimer and monomer, respectively (Figure 3a,b). Thus, we attribute the shorter wavelength emission to the low concentration of monomer present in equilibrium with the excimer, which is the predominant species (see below) but is very weakly fluorescent. The very weak monomer fluorescence indicates that the hairpin dimer remains associated in the excited state, in contrast to the behavior of the PDI foldamers studied by Li et al. which unfold following electronic excitation in organic solvents.[36] Hydrophobic association as well as salt effects (see below) can account for the absence of excited-state dissociation in the case of the hairpin dimers.

Unlike fluorescence which detects only emissive excited states, transient absorption detects all excited molecules with decay times longer than the exciting laser pulse. The transient absorption spectrum of **1** under high salt conditions at 20 °C (Figure 7a) undergoes a time-dependent change in band shape. The band shape after 100 ps is narrower than the initial band shape and is similar to that observed for a cofacial PDI dimer having approximately parallel long axes in organic solvents.[21] The major component of the transient decay has a decay time of 1.5 ns. We tentatively attribute the change in band shape to geometric relaxation of the $^{1*X}PDI_2$ Franck−Condon state, which has a ca. 20° twist angle between PDI long axes, to the parallel geometry. This proposal is consistent with the excited-state potential energy surface for the gas phase PDI dimer derived from a quantum chemical approach proposed by Fink et al.[32] The transient decay dynamics for the hairpin dimer is more fully described elsewhere.[24]

The transient absorption spectrum of **1** under high salt conditions at 70 °C (Figure 7c) displays band maxima at both 654 and 709 nm attributed to the excimer and monomer, respectively. The observation of similar band intensities at short delay times is consistent with the presence of similar concentrations of monomer and dimer at 70 °C, the melting temperature of the dimer (vide infra). The 705 nm monomer band decays more rapidly than the 654 nm excimer band, in accord with the decay times observed for the monomer (Figure 7a) and excimer at 20 °C (Figure 7b).

**Salt and Hairpin Concentration Dependence of the Monomer−Dimer Equilibria.** Both the UV and fluorescence spectra of 1 $\mu$M **1** are dependent upon the concentration of added NaCl (Figures 3 and 4). As previously discussed, spectra obtained in the absence and presence of 1.0 M NaCl are assigned to the hairpin monomer and dimer, respectively. Plots of the mole fraction of dimer vs log [$Na^+$], obtained from the absorption and fluorescence peak intensity ratios are shown in Figure 11.[40] The UV data are considered to be more accurate at high salt concentrations because of the very weak fluorescence under these conditions. A NaCl concentration of ca. 50 mM provides equal concentrations of monomer and dimer and the onset of dimer formation requires a threshold salt concentration of ca. 10 mM.

The effect of NaCl concentration on the monomer−dimer equilibrium is similar to that reported recently for the equilibrium between 14-mer hairpins having a tetranucleotide loop and the corresponding duplexes.[41] However, a higher NaCl concentration (ca. 100 mM) is necessary to provide equal concentrations of the 14-mer hairpin and duplex. The effect of added salt on duplex formation was attributed to an increase in cation condensation about the central region of the duplex, when compared to the disordered loop region of the hairpin.[41] In the case of the PDI-linked hairpin, cation condensation should also increase upon formation of the head-to-head hairpin dimer due to the proximity of the phosphates nearest to the PDI linkers. Higher salt concentration may also confine the large, exposed hydrophobic PDI faces to a smaller volume, a phenomenon known as electrostriction, thus favoring dimer formation.[42] We have observed that added salt enhances the association of pyrene chromophores on the hydrophobic face of a G-quadruplex assembled from four single strands of a G-rich oligonucelotide possessing a 5′-tethered pyrene.[43]

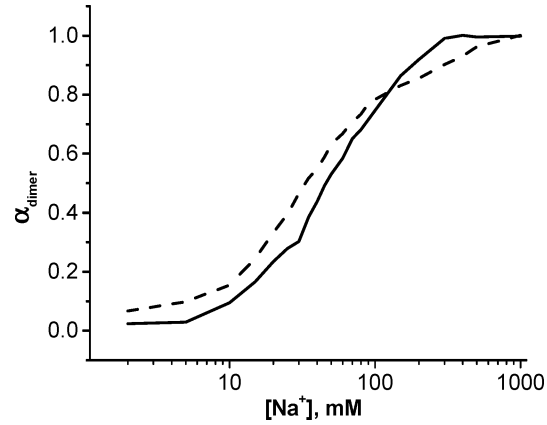


***Figure 11.*** Sodium ion concentration dependence of dimer formation obtained from analysis of absorption (solid curve) and fluorescence (broken curve) spectra data.[40]

For a fixed intermediate value of the salt concentration, increasing the concentration of **1** should increase the dimer/monomer ratio. The association constant for the hairpin dimer formation can be determined using the concentration dependent changes in absorption spectra of conjugate **1** in 10 mM phosphate buffer (pH 7.2) containing 0.1 M NaCl (Figure 2) according to eq 1,

$$\varepsilon(c) = \frac{2Kc + 1 - \sqrt{4(Kc + 1)}}{2K^2c^2}(\varepsilon_f - \varepsilon_a) + \varepsilon_a \qquad (1)$$

where $\varepsilon$ denotes the apparent extinction coefficient obtained from the spectra; $\varepsilon_f$ and $\varepsilon_a$ are the extinction coefficients for the free and the aggregated species respectively; $K$ is the binding constant; and c is the total PDI concentration in the sample.[1,44] The apparent extinction coefficient at 505 nm was fit by nonlinear regression analysis to the isodesmic model which gave a $K_{ass} = 3800 \pm 200\ M^{-1}$ (Figure 2, inset), corresponding to a free energy for dimer formation of ca. −5 kcal/mol in the presence of 0.1 M NaCl. This value is within the range of interaction energies (2−7 kcal/mol) reported for PDI dimers in

(40) The mole fraction of dimer at any concentration of NaCl can be determined from the equation $\alpha_{dim} = (\chi_o - \chi_c)/(\chi_o - \chi_\infty)$, where $\chi_o$ is the ratio $A^{0-0}/A^{0-1}$ (or $I_{549\ nm}/I_{657\ nm}$) in the absence of added salt, $\chi_c$ is the ratio in the presence of added salt, and $\chi_\infty$ is the ratio at infinite (or 1 M) salt concentration.

(41) Nakano, S.; Kirihata, T.; Sugimoto, N. *Chem. Commun.* **2008**, 700–702.
(42) Long, F. A.; McDevit, W. F. *Chem. Rev.* **1952**, *51*, 119–169.
(43) (a) Breslow, R. *Acc. Chem. Res.* **1991**, *24*, 159–164. Zhu, H.; Lewis, F. D. *Bioconjugate Chem.* **2007**, *18*, 1213–1217.
(44) Neumann, B.; Pollmann, P. *Phys. Chem. Chem. Phys.* **2000**, *2*, 4784–4792.

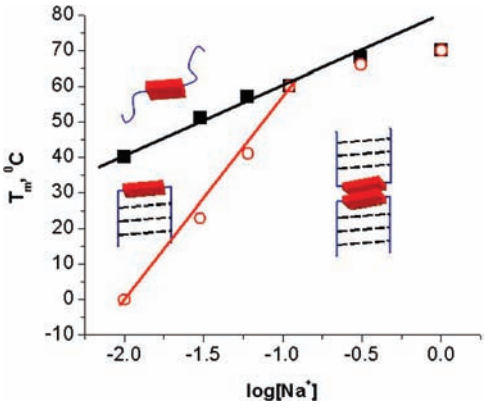


***Figure 12.*** Sodium concentration dependence of the dissociation temperature of the DNA base pairs (black) and the PDI−PDI dimer (red). Structures of the random coil, hairpin, and hairpin dimers illustrate the dominant species for a given combination of temperature and salt concentration.

dichloroethane solution,[31] but is smaller than our calculated value of 13.7 kcal/mol for the nonconjugated PDI dimer in water (Figure 10b). This difference may reflect both the electrostatic repulsion between the two hairpins and the exposure of only two PDI faces to water upon dissociation of the hairpin dimer vs four in the nonconjugated dimer.

**Hairpin and Hairpin Dimer Thermal Dissociation.** The dissociation of the monomer and dimer base pair domains can be monitored using the 260 nm thermal dissociation profiles and dissociation of the PDI dimer can be monitored using the $A^{0-0}/A^{0-1}$ band intensity ratios (Figure 3c,d). The 260 nm UV and CD thermal dissociation profiles for the monomer hairpin **1** in the absence of added salt are consistent with a simple two state melting process (Figures 3c and S3a). Fitting of the 260 nm thermal dissociation profile provides values of $T_m = 40$ °C and $\Delta H° = -28$ kcal/mol.[45] The salt dependence of $T_m$ for duplex oligonucleotides are expected to display a log [$Na^+$] dependence for salt concentrations up to ca. 0.2 M, with a decrease in slope at higher salt concentrations.[46−48] A plot of our 260 nm and $A^{0-0}/A^{0-1}$ $T_m$ data vs log [$Na^+$] (Figure 12, black line) is linear for concentrations between 10 mM and 0.32 M, indicating that hairpin dimer formation does not influence the base pair melting process. The slope of this line ($ST_m = dT_m/d \log[Na^+]$) is 18 °C, similar to the value expected for a duplex with low G−C base pair content.[48] Smaller values of $ST_m$ are observed for hairpins having oligonucleotide loops, as a consequence of the electrostatic interactions of the counterion with the bases in the loop.

The plot of the $A^{0-0}/A^{0-1}$ band intensity ratio data displays a change in slope at a NaCl concentration of ca. 100 mM (Figure 12). At lower salt concentrations, values of $T_m$ are smaller than those for 260 nm melting and are more strongly dependent upon salt concentration, having a value of $ST_m = 57$ °C. The larger slope is indicative of a significantly smaller enthalpy of dissociation for the PDI dimer than for base pairs melting, in accord with the value of 5 kcal/mol estimated for the free energy of dimerization in 0.1 M NaCl. At higher salt concentrations, values of $T_m$ obtained from the $A^{0-0}/A^{0-1}$ band intensity ratio are the same as those for 260 nm melting. This suggests that base pair melting may trigger PDI dissociation at higher salt concentrations. Values of $T_m$ for 100 mM and 1.0 M salt are similar to those for monomeric stilbenedicarboxamide-linked hairpins at these salt concentrations,[18] indicating that PDI hydrophobic association does not have a significant effect on base pair melting at higher salt concentrations.

The UV, CD, and fluorescence thermal dissociation profiles in the presence of 1 M NaCl (Figures 3d, S3b,c, and 5 inset, respectively) all show evidence of premelting at temperatures below the transitions assigned to concomitant melting of the base pairs and PDI dimer dissociation. Since premelting behavior is observed in both the base pair and PDI regions of the UV and CD spectra, we conclude that the hairpin dimer undergoes temperature-dependent structural changes prior to the concomitant melting of the base pairs and PDI dimer.[47] However, the nature of these changes cannot be determined from the available spectroscopic data.

It is interesting to compare the temperature dependence of the hairpin monomer−dimer equilibrium (Figure 12) with the behavior of the intramolecular PDI dimers and oligomers connected with oligonucleotide chains studied by Wang et al.[11] These conjugates undergo increased PDI aggregation upon heating in aqueous solution; however, analogues possessing linkers soluble in organic solvents do not display thermophilic folding.[11,35,36] The unusual temperature dependence of the conjugates studied by Wang et al. is attributed to a positive enthalpy for intramolecular hydrophobic PDI association which is observed only in aqueous solution. In agreement with their observations, we find that base pair melting in dumbbells having PDI linkers at both ends is assisted by intramolecular PDI−PDI dimerization.[49]

**Concluding Remarks.** Hydrophobic association of the PDI-linked bis(oligonucleotide) conjugate **1** in aqueous solution to form a hairpin dimer structure (Chart 1) is dependent upon salt concentration and temperature (Figure 12), as well as the concentration of **1** (Figure 2, inset). The data shown in Figure 12 demonstrate that hairpin dimer melting at low salt concentrations is a two-stage process; dimer dissociation occurring at lower temperatures than base pair melting. The observation of similar base pair and PDI dimer melting temperatures at higher salt concentrations suggests that formation of a stable hairpin dimer requires an intact base-pair domain, as well as the presence of added salt and that base pair melting triggers dissociation of the PDI−PDI dimer. We note that Figure 12 provides an approximate phase diagram for conjugate **1**, the dominant species being the hairpin monomer at low temperatures and low salt concentrations, the hairpin dimer at low temperatures and high salt, and the random coil structure at high temperatures.

The hairpin monomer and dimer display distinctive UV, CD, fluorescence, and transient absorption spectra. The decrease in the $A^{0-0}/A^{0-1}$ band intensity ratio in the UV spectrum and the appearance of red-shifted excimer fluorescence upon dimer formation is similar to numerous prior reports for PDI dimers and aggregates in nonaqueous solution.[1,2,44] However, the pronounced long-wavelength tails in the absorption spectra and corresponding CD bands are unique to the hairpin dimers and suggest the presence of electronic interactions between the PDI chromophores and adjacent base pairs. The transient absorption spectra of the monomer and dimer singlet states are also highly distinctive, the monomer having a relatively narrow symmetric

(45) McDowell, J. A. *MeltWin 3.5* **2001**, .
(46) Schildkraut, C.; Lifson, S. *Biopolymers* **1968**, *3*, 195–208.
(47) Cantor, C. R.; Schimmel, P. R. *Techniques for the Study of Biological Structure and Function*; W. H. Freeman: New York, 1980.
(48) Shkel, I. A.; Record, M. T. *Biochemistry* **2004**, *43* (22), 7090–7101.
(49) Zhang, Y. Ph. D. Thesis, Northwestern University, 2007.

band centered at 705 nm band and the dimer having a broadband which evolves to a narrower band at 654 nm. The time-dependent change in the dimer transient spectrum is tentatively attributed to a change in the dimer geometry from nonparallel in the ground-state to parallel in the excited state. Studies of the structures and excited-state behavior of other PDI oligonucleotide conjugates are in progress in our laboratories.

**Acknowledgment.** This research is supported by a grant from the National Science Foundation, Collaborative Research in Chemistry for the project DNA Photonics (CHE-0628130 to G.C.S., F.D.L., and M.R.W.). D.M.T. and X.Z. and the X-ray scattering experiments at the Advanced Photon Source, beamline 12-ID were supported by the Office of Basic Energy Sciences, DOE under Contract No. DE-AC02-06CH11357. The authors gratefully acknowledge Dr. Soenke Seifert for his expert help in setting up the X-ray scattering measurements.

**Supporting Information Available:** Materials and Methods section, fluorescence excitation spectra (Figure S1), concentration-dependent fluorescence spectra (Figure S2), CD melting curves (Figure S3), Guinier plot for the hairpin dimer (Figure S4), calculated rotational potential for the hairpin dimer (Figure S5), PDI dimer structure in PMF calculation (Figure S6), and a description of the potential mean force calculations. This material is available free of charge via the Internet at http://pubs.acs.org.

JA900347T